Riehl and Malkus Revisited: The Role of Cloud-Radiative Effects

Michael R. Needham[1], David A. Randall[1]

[1]Department of Atmospheric Science, Colorado State University, Fort Collins, CO, USA

Key Points:

- Cloud-longwave feedbacks discussed in previous studies appear to be examples of a more general cloud feedback driven by the ACRE
- Warm, humid regions export energy and import moisture in a way similar to the ITCZ
- The ACRE as a function of CRH is nearly independent of the SST

Corresponding author: Michael R. Needham, `m.needham@colostate.edu`

Abstract

The intertropical convergence zone (ITCZ) exports energy and imports moisture in a way that has been well-understood for decades. By analyzing a set of uniform, non-rotating aquaplanet simulations we show that energy export and moisture convergence are general characteristics of warm humid regions, and not just of the ITCZ. Using an analysis method based on the column relative humidity, we find that the absorption of longwave radiation by clouds provides the necessary energy source to balance the horizontal energy export out of humid regions. The longwave absorption also induces a thermally direct circulation which lifts water vapor and leads to low-level moisture convergence into regions that are already quite humid. This feedback is similar to other cloud-longwave feedbacks which have been previously studied.

1 Introduction

The top of atmosphere radiation balance indicates that the tropics are a source of energy for the rest of the atmosphere. Our understanding of the resulting tropical energy export is due largely to the germinal work of Riehl and Malkus (1958, hereafter RM58). They performed an energy and moisture budget analysis of the Intertropical Convergence Zone (ITCZ, which they called the equatorial trough zone), a narrow belt of moisture convergence and enhanced precipitation that sits a few degrees north of the equator on average (Byrne et al., 2018). Using radiosonde observations from a few dozen sites around the tropics, as well as estimates of the zonal-mean radiative imbalance of the northern hemisphere as a function of the seasons, RM58 showed a net outflow of energy out of the ITCZ, and a net convergence of moisture into the ITCZ. The net energy outflow implies an energy within the ITCZ. The energy transport is accomplished through the upper-level export of dry static energy (s, the combination of potential energy and enthalpy), while the moisture transport is accomplished by the low-level import of water vapor.

In addition, RM58 understood that the low-level moisture import and upper-level energy export implies an upward flux of energy within the ITCZ. There were several possible mechanisms that could accomplish this; diffusion, ascent within synoptic disturbances, or ascent within protected convective updrafts. RM58 observed the now familiar tropical profile of moist static energy (h, the combination of s and latent energy) which is uniform with height through the boundary layer, decreases with height above the bound-

ary layer and then increases with height above a mid-tropospheric minimum due to the increase of potential energy. The existence of the minimum led RM58 to eliminate the first two mechanisms: diffusion would be unable to transport energy upward above the minimum because that would go against the energy gradient, and large-scale ascent would eliminate the minimum itself because h is conserved following an air parcel. Instead, RM58 hypothesized that protected convective updrafts could travel through the mid-tropospheric minimum to transport energy from the moist boundary layer to upper levels, where it could be transported poleward by the Hadley cells. In short, RM58 concluded first that the ITCZ is a source of energy and a sink for moisture due to the export of energy and the import of water vapor, and second that convective-scale ascent is key to the necessary vertical transport.

Neelin and Held (1987) studied the ITCZ in a manner similar to RM58. They described how low-level mass convergence in the tropics must, on-average, occur in locations where the atmosphere is gaining energy. That is, a net convergence of energy in the atmosphere drives low-level moisture convergence into the ITCZ, as discussed by RM58. The atmospheric energy convergence emphasized by Neelin and Held (1987) could plausibly come from one or more of several sources. These include fluxes of latent and sensible energy from the surface (together, the surface flux of moist static energy), as well as the flux convergence of longwave and shortwave radiation.

A large body of work has explored the particular importance of the absorption of radiation by clouds on the atmosphere. Termed the atmospheric cloud radiative effect (ACRE), this has been shown to greatly impact large-scale phenomena such as the ITCZ and the Hadley cells (Slingo & Slingo, 1988; Randall et al., 1989). Sherwood et al. (1994) investigated the influence of the ACRE on tropical circulations in an atmospheric global circulation model. They found that removing the ACRE above 600 hPa led to a reduction in the strength of the hadley and walker circulations. Similar results have been found in more recent studies utilizing updated GCMs, which have also noted the role of ACRE in determining the width of the ITCZ, reducing the double-ITCZ bias, and strengthening the precipitation associated with various tropical phenomena (Li et al., 2015; Harrop & Hartmann, 2016; Popp & Silvers, 2017; Albern et al., 2018; Voigt & Albern, 2019; Benedict et al., 2020; Medeiros et al., 2021).

Sherwood et al. (1994) also described a positive feedback between ACRE and cloudiness, in which cloud radiative heating drives rising motion which favors cloud formation that in turn leads to further cloud radiative heating. This type of tropical cloud-longwave feedback has recently received a lot of attention in the several different contexts. Wing and Emanuel (2014) introduced a new method for investigating the feedbacks that govern convective self-aggregation using the spatial variance of the frozen moist static energy. Among other mechanisms discussed, they found that the longwave flux convergence was strongly positive in extremely humid regions of a cloud resolving model without rotation, and represents a strong positive feedback for maintaining an aggregated state. In rotating simulations of radiative-convective equilibrium (Arnold & Randall, 2015; Khairoutdinov & Emanuel, 2018), a similar variance analysis shows the important role of cloud-longwave feedbacks in maintaining a disturbance that behaved much like the Madden-Julien Oscillation (MJO). Recently, Benedict et al. (2020) used cloud-locking simulations to show that removing the ACRE weakened the MJO, highlighting the importance of the interactions between clouds and longwave radiation. Using the same cloud locking simulations as well as a set of COOKIE experiments (Stevens et al., 2012) that made clouds invisible to radiation, Medeiros et al. (2021) found that removing cloud-radiative feedbacks weakened tropical precipitation by reducing the frequency of extreme precipitation events. Work by Ruppert et al. (2020) has also shown that this type of feedback is important for regulating the intensification of tropical cyclones.

These and other tropical convective phenomena are strongly coupled to precipitation, which in turn is strongly coupled to humidity (Raymond, 2000). Bretherton et al. (2004) showed that the mean tropical precipitation rate can be described as a simple exponential function of the column relative humidity (CRH, the ratio of the actual to the observed water vapor path, alternatively known as the saturation fraction). This has been well supported by later studies (Raymond & Zeng, 2005; Raymond et al., 2009; Rushley et al., 2018; Powell, 2019; Wolding et al., 2020). Analysis suggests that this relationship may be better understood by considering the concurrent evolution of precipitation and humidity, in which grid cells slowly build up water vapor up to some critical value, at which point they quickly lose water vapor to precipitation (Peters & Neelin, 2006; Neelin et al., 2009; Wolding et al., 2020). In a recent paper, Needham and Randall (2021) demonstrated a nonlinear relationship between the mean ACRE and the CRH that is similar to the well-documented relationship between precipitation and CRH. They further sug-

gested a connection between the two relationships in the form of a cloud-longwave feedback driven by the longwave ACRE.

In this study, we emulate the budget analysis of RM58 using a set of idealized aquaplanet simulations performed in the absence of rotation with uniform sea surface temperatures (SSTs). We find that the main conclusions of RM58 hold in our idealized simulations even though they do not contain an ITCZ or any other regions with a time-mean convergence of moisture. This suggests that all humid regions of the tropics may function like the ITCZ, in that they export energy and import moisture. Furthermore, we observe a cloud-longwave feedback that is driven by the ACRE in humid regions. This feedback strongly resembles those emphasized in previous studies, as discussed above.

Section 2 provides an overview of the model simulations used in this study, and includes a discussion of an analysis method utilizing the CRH that will be used extensively to separate dry and humid regions. In section 3 we show that the ACRE becomes large in humid regions, and find support for the main conclusions of Needham and Randall (2021). The moisture and energy budgets of the simulations are analyzed using the CRH method in section 4. The budget analyses demonstrate that the simulated humid regions export energy and import moisture, like the ITCZ. Section 5 shows that the characteristic minimum in the vertical profile of moist static energy is weakened in the most humid regions. Further analysis shows that dry regions of the simulations are characterized by weak large-scale subsidence, while humid regions are characterized by strong convection as well as environmental ascent. This ascent appears to be responsible for weakening the vertical gradient of moist static energy, and the source of the rising motion is determined to be ACRE. This leads to the identification of a radiatively driven moisture feedback, in which strong ACRE in humid regions drives low level moisture convergence and large-scale ascent which lifts water vapor, leading to the formation of more clouds. Conclusions are presented in section 6.

2 Data and Methods

2.1 Model simulations

The model output used in this study come from a set of simulations performed with a super-parameterized version of the Community Atmosphere Model 4 (CAM4), and are the same simulations analyzed in a recent paper by Jenney et al. (2020), where they are

described in detail. The model uses a $0.9° \times 1.25°$ horizontal grid with 26 levels and covers the entire globe. The three simulations were configured following the protocol of the Radiative-Convective Equilibrium Model Intercomparison Project (Wing et al., 2018, hereafter RCEMIP), and were included in the preliminary analysis of that project (Wing et al., 2020). The RCEMIP simulations were performed without rotation and without land. Insolation was held uniform in time and space, and each of the three simulations had a uniform sea surface temperature (SST) of 295 K, 300 K, or 305 K. Our results are based on an analysis of 30 days of hourly mean data from the fourth simulated year in each simulation. We focus on the 300 K simulation, but nearly identical conclusions were reached when the analysis was repeated for the other two simulations.

The super-parameterized version of CAM4 replaces the traditional convective parameterization with a two dimensional cloud resolving model (the System for Atmospheric Modeling, described in Khairoutdinov and Randall (2003)) embedded within each GCM grid cell. The CRM uses a 4 km horizontal grid spacing with 32 columns and its 24 model levels are aligned with the bottom 24 levels of the GCM. The CRM allows for the explicit simulation of convective-scale dynamics, and more accurately represents small-scale processes by parameterizing cloud microphysics, radiation, and other processes on the finer CRM grid. Heating and drying rates are averaged across the CRM and are passed back to the GCM. A more detailed discussion of super-parameterization is provided by Randall et al. (2016).

2.2 Analysis using the Column Relative Humidity

The RCEMIP simulations lack the coriolis effect and meridional temperature gradient which give rise to an ITCZ in the real tropics and in more realistic simulations. These uniform conditions indicate that there should be no regions characterized by a time mean convergence of moisture. However this does not indicate that water vapor is uniform in these simulations. Instead, at any given moment the RCEMIP simulations contain a few large, heavily precipitating regions which slowly migrate within a broader dry environment. Snapshots showing the OLR, precipitable water, and 500 hPa vertical velocity at a given moment for the 300 K simulation are shown in Fig. 1, and a movie showing the evolution of the precipitable water is included as a supplemental file.

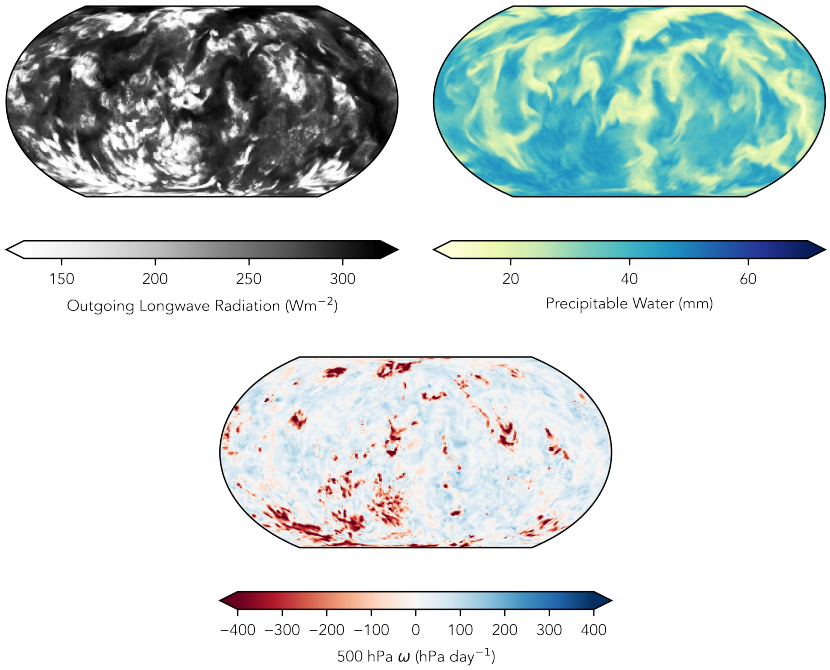

Figure 1. Outgoing longwave radiation (**top left**) precipitable water (**top right**), and vertical velocity across the 500 hPa surface (**bottom**), at the same arbitrary timestep for the 300 K simulation.

To investigate the various ways that the dry and humid regions interact, we will analyze the three RCEMIP simulations using the column relative humidity,

$$\mathrm{CRH} = 100\% \times \frac{\int_{p_t}^{p_s} q dp}{\int_{p_t}^{p_s} q^*(T) dp}. \tag{1}$$

Model diagnostics are analyzed by taking the area weighted average value of a field using only those grid cells with CRH within a bin of width 2%, and then repeating for all bins between 0% and 100% CRH. Similar analyses using the CRH have been used previously (e.g., Bretherton et al. (2005); Wing and Emanuel (2014); Jenney et al. (2020)), and the method used here is identical to that of Needham and Randall (2021).

The curves in Fig. 2 show the probability density function (PDF) of the CRH for each of the three RCEMIP simulations, with the curve for the 300 K emphasized using

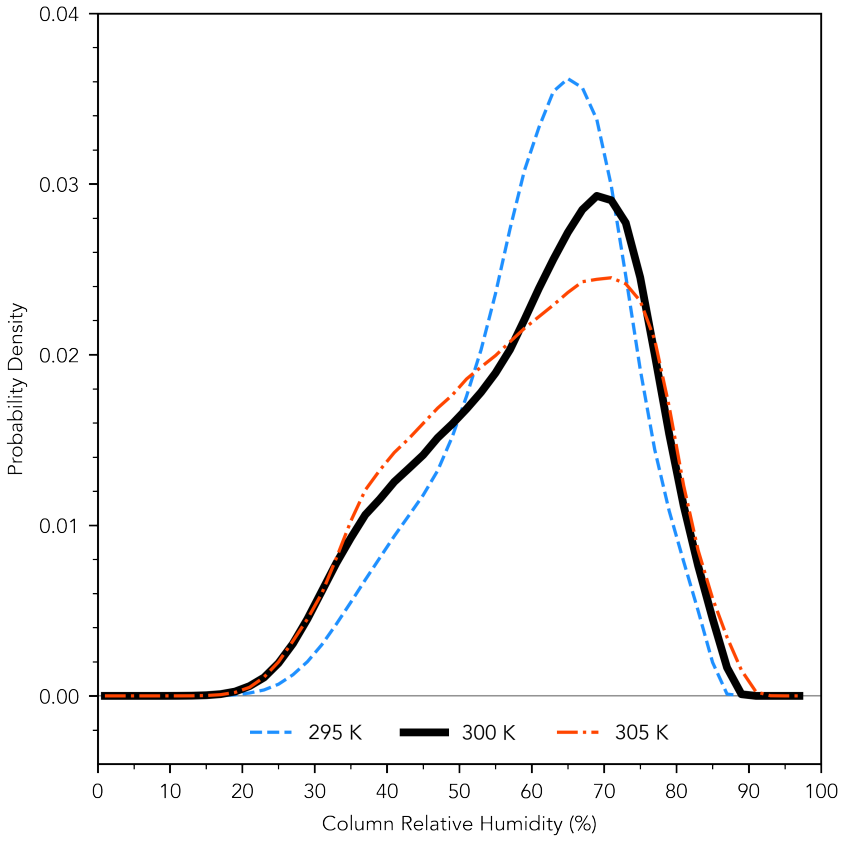

Figure 2. Probability density function of CRH for each of the three RCEMIP simulations.

Table 1. Summary statistics of the CRH for each of the simulations, as well as domain-average values of the top of atmosphere CRE and the ACRE.

	Mean (%)	σ (%)	Skewness	Kurtosis	Mode (%)	CRE (Wm^{-2})	ACRE (Wm^{-2})
295 K	60.753	11.947	-0.489	-0.176	64.875	-14.142	22.641
300 K	59.910	15.075	-0.446	-0.703	69.375	-18.858	23.766
305 K	59.381	15.127	-0.258	-0.776	70.875	-16.979	26.121

a heavy black line. The PDFs show that each of the simulations has a peak in the distribution of CRH between 60% and 75%. As the SST increases, the PDFs become wider and shorter, which indicates more extremely dry and extremely humid grid cells in the 305 K simulation compared to the 295 K simulation. Each of the PDFs goes to zero near 20% on the low end and near 90% on the high end. Summary statistics for the CRH are included in Tbl. 1.

3 Cloud Radiative Effect Versus Column Relative Humidity

The CRH binning method was used to calculate the mean vertically-integrated full-sky and clear-sky radiative heating rates for each of the three RCEMIP simulations, which are shown in the top row of Fig. 3. The full-sky rate (thick lines) is the total heating rate due to radiation, while the clear-sky rate (thin lines) is the heating rate that would occur if clouds were made invisible to radiation, but leaving only the radiative effects of temperature, humidity, aerosols, and any radiatively active gases. Panel a illustrates that the longwave heating rates are negative in both dry and humid regions. As the CRH increases, the increase in water vapor leads to more radiative cooling up to about 60%, at which point the cooling rate begins to strongly decrease with increasing CRH. This decrease in magnitude does not occur in the same way for the clear-sky rate so that the ACRE, calculated as the difference between the full-sky and clear sky rates (and shown in panel d) begins to increase dramatically in humid regions. As the SST increases from 295 K to 300 K and 305 K, both the full-sky and clear-sky cooling increase in magnitude. However this increase appears to occur at roughly the same rate, so that the ACRE remains unchanged.

The shortwave heating rates are shown in panel b, and increase only slightly as the CRH increases, compared to the longwave. The full-sky and clear-sky rates are very close

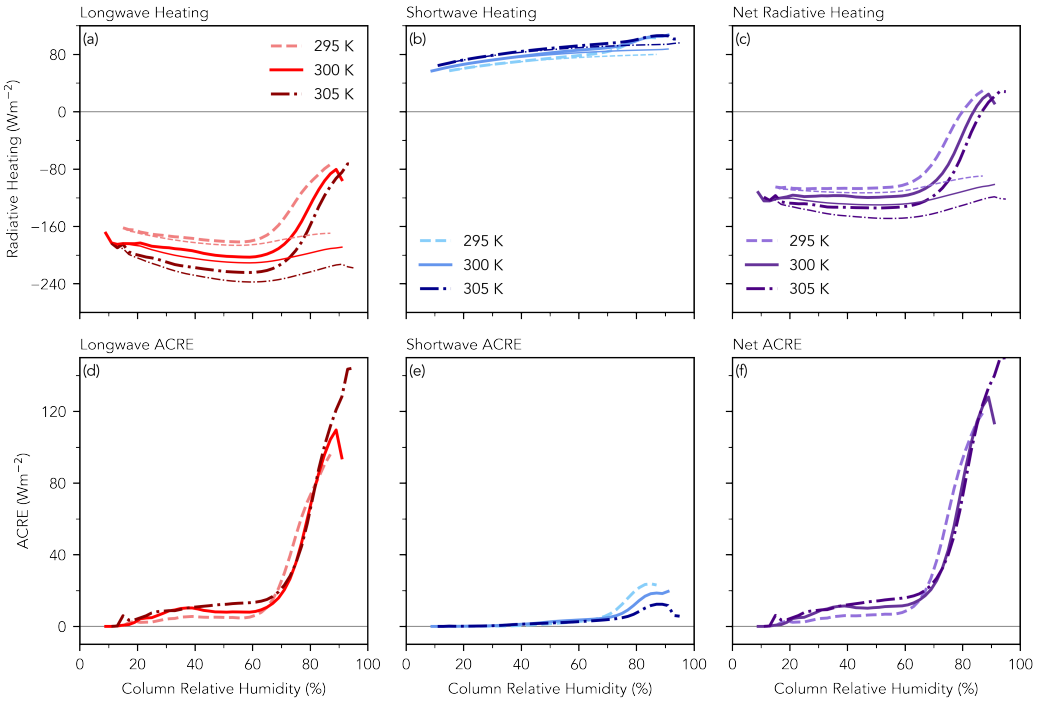

Figure 3. **Top Left:** Integrated full-sky (thick lines) and clear sky (thin lines) longwave heating rates for each of the RCEMIP simulations as a function of the column relative humidity. **Top Middle** and **Top Right:** Same as **Top Left**, but for shortwave and net radiative heating rates. **Bottom Row:** Same as **Top Row**, but for the ACRE.

together, indicating that clouds don't account for a large amount of shortwave absorption. Consequently, the shortwave ACRE (panel e) is nearly zero in dry regions, and is small in humid regions compared to the longwave effect. Together, the net ACRE is largely determined by the longwave effect, consistent with previous work (Slingo & Slingo, 1988; Allan, 2011). This is in contrast to the CRE at the top of the atmosphere, which includes a strong shortwave effect (Ramanathan et al., 1989; Harrison et al., 1990; Hartmann & Berry, 2017). The mean longwave ACRE is small in dry regions and begins to increase rapidly as the CRH exceeds a threshold near 70%. A key conclusion of Needham and Randall (2021) was that the mean ACRE for a particular CRH was nearly identical in different regions of the tropics. The same conclusion is reached here in the context of these idealized simulations: as the SST increases, the ACRE at a given CRH appears to remain nearly unchanged. Changes to the ACRE in a warmer climate may then be due only to changes in the CRH, although this hypothesis needs further study. Another important conclusion from Fig. 3 is that the net radiative heating rate changes sign to become positive in extremely humid regions (panel c). This point is discussed further in section 5

Fig. 4 shows the CRE binned by the CRH for the 300 K simulation (similar plots were generated for the other two simulations). The panels in Fig. 4 include the median (solid line) as well as the mean (dotted line), and the shading represents the range between the 25th and 75th percentiles within each CRH bin. The top row of the figure shows the longwave, shortwave, and net cloud radiative effects at the top of atmosphere as functions of the CRH. The middle row shows the CRE at the surface, while the bottom row shows the ACRE, calculated as the difference between the two. Note that the bottom row uses a different scale on the y-axis than the scale used with the top and middle rows.

The longwave CRE at the top of atmosphere (panel a) is small in dry regions but begins to increase as the CRH exceeds a threshold of about 70%. The shortwave CRE (panel b) behaves qualitatively the same as the longwave effect, but is of larger magnitude and of opposite sign. As the negative shortwave effect is larger than the positive longwave effect, the net CRE at the top of atmosphere is negative in all regions, and reaches its largest magnitude in humid regions, as expected. At the surface the longwave effect (panel d) is small and positive, capturing the enhanced longwave emission to the surface from the cloud bases. The shortwave effect in panel e behaves almost identically to the shortwave effect in panel b, which shows that the effect of clouds on shortwave ra-

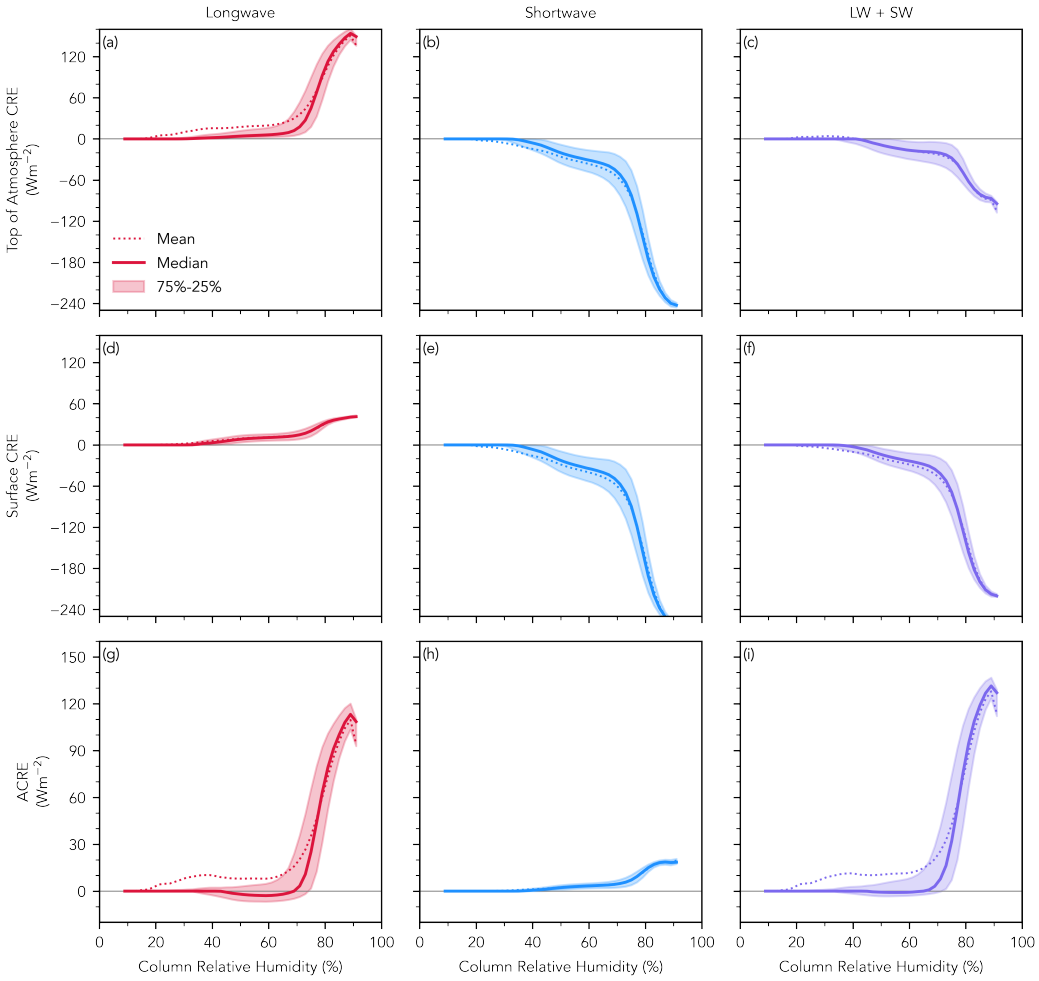

Figure 4. **a:** Longwave cloud radiative effect at the top of the atmosphere, binned by the CRH. The dotted line shows the area-weighted average CRE in each CRH bin, the solid line shows the 50th percentile, and the shading shows the range between the 25th and 75th percentiles. **b** and **c:** Same as **a**, but for the shortwave and net CRE. **d-f:** Same as **a-c**, but for the surface CRE. **g-i:** Same as **a-c**, but for the ACRE.

diation is felt mostly at the surface, rather than in the atmosphere itself, and is due to the enhanced cloud albedo. The net CRE at the surface is, like the top of atmosphere effect, largely determined by the shortwave (panel f).

In panel g of Fig. 4, the longwave ACRE is skewed in dry regions, with the median value near zero while the mean value exceeds the 75^{th} percentile. This indicates that in dry regions clouds usually have little to no effect, with the exception of a few clouds which absorb a large amount of longwave radiation. This may be the effect of high cirrus clouds which are advected away from humid regions and into dry regions, and trap longwave emission from the surface and lower levels of the atmosphere. In humid regions the distribution becomes much less skewed as the mean and median are nearly on top of one another. The shortwave ACRE (panel h) reaches its largest magnitude in humid regions, but is still very small compared to the surface shortwave CRE, which again shows that clouds reflect much more sunlight than they absorb. Because the shortwave effect is so small, the net ACRE (panel i) is dominated by the longwave component, and is characterized by the same skewed distribution in dry regions and rapid strengthening in humid regions. However, the net ACRE is slightly larger than the longwave ACRE due to the positive shortwave contribution.

Fig. 4 shows that in extremely humid regions the net CRE at the top of atmosphere is dominated by the shortwave effect. At first glance this may appear to conflict with previous studies that have found that the net top of atmosphere CRE nearly cancels in the tropics (Ramanathan et al., 1989; Hartmann & Berry, 2017). We emphasize that the shortwave dominance occurs only in extremely humid regions where the CRE becomes large. In most of the domain the CRH does not exceed 80%, so these humid grid cells do not factor into the domain-average CRE with too much weight: this can be seen in Tbl. 1 where the CRE does not exceed 20 Wm^{-2} for any of the three simulations. When the CRE is decomposed into surface and atmospheric components, the shortwave effect acts primarily at the surface, while the longwave effect determines the ACRE. Panel i shows that the net ACRE can be a large heat source for the atmosphere, on the order of 100 W m^{-2} in very humid regions. To see the impact of this atmospheric energy convergence, in the next section we perform an analysis of the energy and moisture budgets, following the lead of Riehl and Malkus (1958).

4 Budgets of Energy and Moisture

To interpret the budget analyses, it is important to keep in mind the differences between the RCEMIP simulations and the real earth, which were mentioned above in Section 2. The RCEMIP simulations are performed without rotation and without meridional SST gradients, and they are forced with spatially uniform insolation. This means that while the temperature and lack of Coriolis acceleration lead to "tropical" conditions, the simulations do not have a true"tropics" in the sense that there are no regions characterized by a time-mean surplus of radiative energy that must be exported to higher latitudes. The absence of rotation also means that a structure like the ITCZ does not exist in the RCEMIP simulations. More generally, there are no regions in these simulations that are characterized by a time-mean convergence or divergence of moisture or energy. A skeptical reader may ask whether these differences complicate drawing inferences of the real atmosphere, especially on the interplay between humid and dry regions given the convectively-aggregated state. As part of a M.S. thesis, Needham (2021) found that these results are replicated when the analysis is repeated for a set of aquaplanet simulations with rotation, a meridional SST gradient, and a diurnal cycle.

We now turn to an analysis of the budgets of energy and moisture in the RCEMIP simulations, beginning with energy. The time-mean energy balance of an atmospheric column can be understood in terms of the convergence of energy into that column (Neelin & Held, 1987), written as

$$-\int_0^\infty \nabla_H \cdot (\rho \mathbf{V} h) dz = \nabla \cdot (\mathbf{R} + \mathbf{F}_h). \tag{2}$$

Here, $\mathbf{R}$ and $\mathbf{F}_h$ represent the flux of radiation and moist static energy into the column, from the surface and the top of the atmosphere. As we are currently unconcerned with the vertical structure, Eq. 2 can be rewritten as

$$Q = (LW + SW)_{\text{toa}} + (LW + SW)_{\text{sfc}} + SH + LE. \tag{3}$$

In words, the atmospheric energy flux convergence Q depends on the fluxes of longwave and shortwave radiation across the top of the atmosphere, the fluxes of longwave and

shortwave radiation across the surface, and the surface flux of moist static energy (MSE, the combination of sensible heat and latent energy).

The terms comprising the energy balance for the 300 K simulation are shown in Fig. 5, where they have been binned by the CRH similar to Figs. 3 and 4. Panel a shows longwave flux across the top of atmosphere and surface as well as the net convergence of longwave radiation into the atmosphere. Both of the fluxes decrease in magnitude as the CRH increases, but the magnitude of the top of atmosphere flux begins to drop precipitously when the CRH exceeds about 70%. As discussed in reference to Figs. 3 and 4, the change in the longwave convergence is due to the ACRE. The shortwave fluxes are shown in panel b. Both the top of atmosphere and surface terms show a decrease in magnitude in humid regions. In contrast to the longwave, this does not represent a strong convergence of shortwave radiation, but rather represents the enhanced cloud albedo effect which reflects solar radiation back to space. The atmospheric shortwave convergence shows little dependence on the CRH. Similarly, the surface flux of moist static energy, shown in panel c, does not change much as the CRH increases.

The sum of the longwave, shortwave, and MSE terms is shown as the thick orange line in panel d, which represents the net convergence of energy into the atmosphere as a function of the CRH (Q in Eq. 3). In dry regions Q is near zero or slightly negative, as shortwave heating and surface fluxes are balanced by longwave cooling. In humid regions the longwave term becomes small while the shortwave and MSE terms do not depend much on the CRH. This leads to an increase in Q which corresponds to a strong vertical convergence of energy into the atmosphere. As discussed previously (Fig. 3) the full-sky longwave heating becomes weak in humid regions while the clear-sky heating does not. This indicates that the increase in Q is due to a strong longwave ACRE.

Because the energy budget was computed over the entire sphere, positive Q in humid regions and negative Q in dry regions implies an export of energy out of humid regions and into dry regions. Positive Q also implies low-level horizontal mass convergence into humid regions (Neelin & Held, 1987), which has a strong impact on the moisture balance. The time-mean integrated moisture convergence of the atmosphere is given by

$$-\int_0^\infty \nabla_H \cdot (\rho \mathbf{V} q) dz = P - E, \tag{4}$$

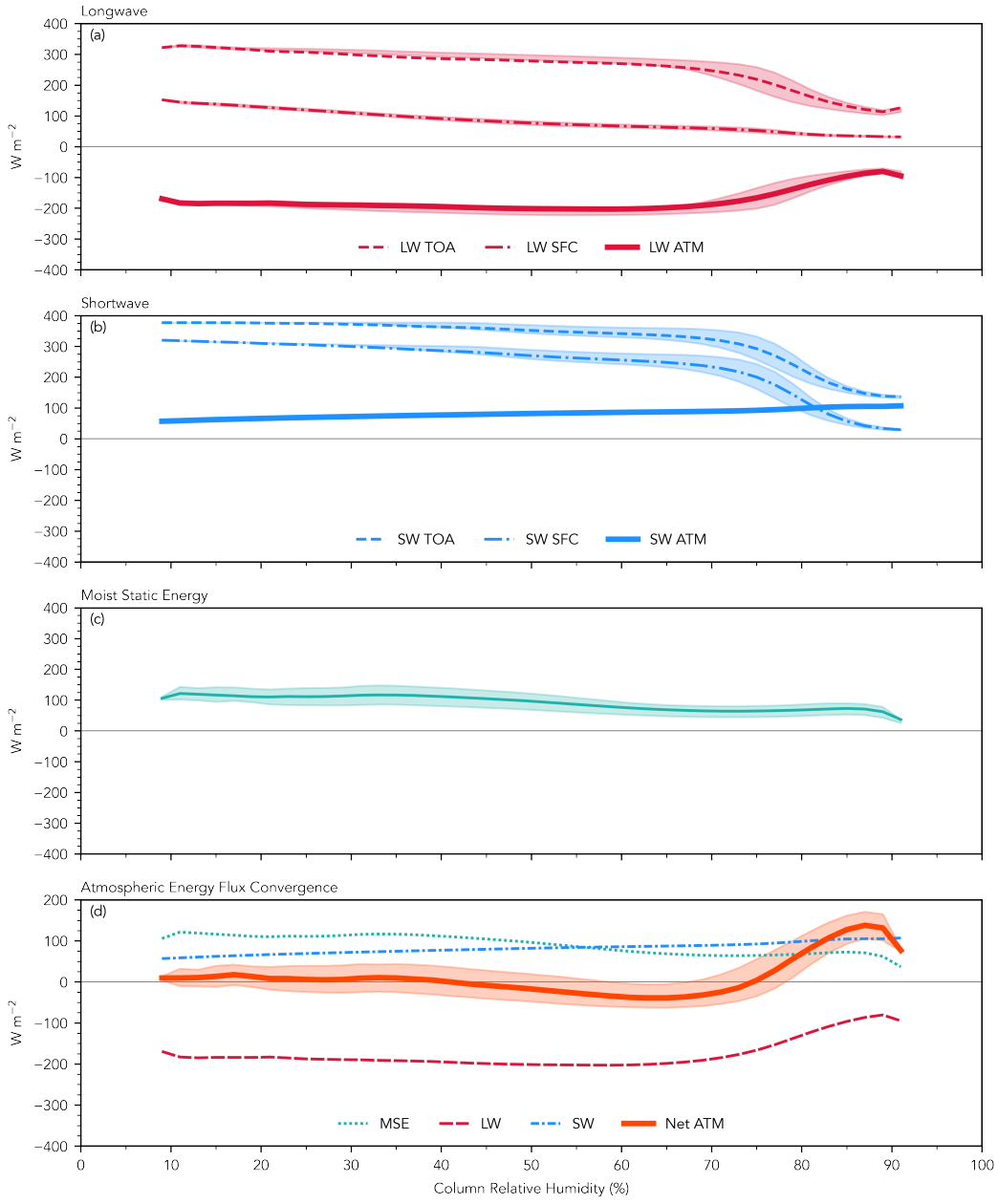

Figure 5. Atmospheric energy budget binned by the column relative humidity, decomposed into contributions from **a:** longwave radiation, **b:** shortwave radiation, and **c:** surface fluxes of moist static energy. The contributions from each of these terms to the total budget are shown in panel **d**.

where P and E represent the rates of precipitation and evaporation. In Eq. 4 we have assumed no long-term storage of moisture in the atmosphere. This leads to a simple water cycle in which moisture enters the atmosphere through evaporation, is transported through dynamic processes, and then exits the atmosphere, likely in another location, as precipitation.

The moisture budget for the 300 K simulation is shown in Fig. 6. Panel a shows the mean and median precipitation rate binned by the CRH, as well as the range between the 25th and 75th percentiles. As expected, the precipitation rate depends exponentially on the CRH (Bretherton et al., 2004), and begins to increase rapidly beyond 70% to 80%. The separation between the mean (dotted line) and median (dashed line) precipitation shows that the distribution is skewed, with a large number events with little or no precipitation and a few downpour events. In contrast to the precipitation rate, the evaporation rate (panel b), shows little dependence on the CRH. The mean evaporation rate ranges between 2 to 6 mm day^{-1} while the precipitation rate can exceed 50 mm day^{-1} in extremely humid regions. This shows that the moisture convergence calculated from Eq. 4 is primarily associated with the precipitation rate.

The budgets of energy and moisture allow us to draw two general conclusions about humid tropical regions. First, humid regions are characterized by a strong longwave ACRE which leads to a net vertical convergence of energy into the atmosphere. This then implies a horizontal export of energy out of the humid regions. Second, humid regions are characterized by moisture convergence against the moisture gradient which then leads to enhanced precipitation. We emphasize again that the energy export and moisture import in humid regions are not the result of rotation or SST gradients, which are not included in the RCEMIP simulations. Instead they are a general characteristic of warm humid regions. It is interesting to note that these conclusions mirror those of RM58, who found that the ITCZ is a region of intense energy export as well as up-gradient moisture transport. RM58 presented their work in a time when the importance of radiative heating was not fully appreciated. They speculated that the energy export out of the ITCZ might be fueled by surface energy fluxes. Our results (Fig. 5) suggest that instead the ACRE is the primary heat source. It appears that all humid regions of the tropics behave like the ITCZ in these ways.

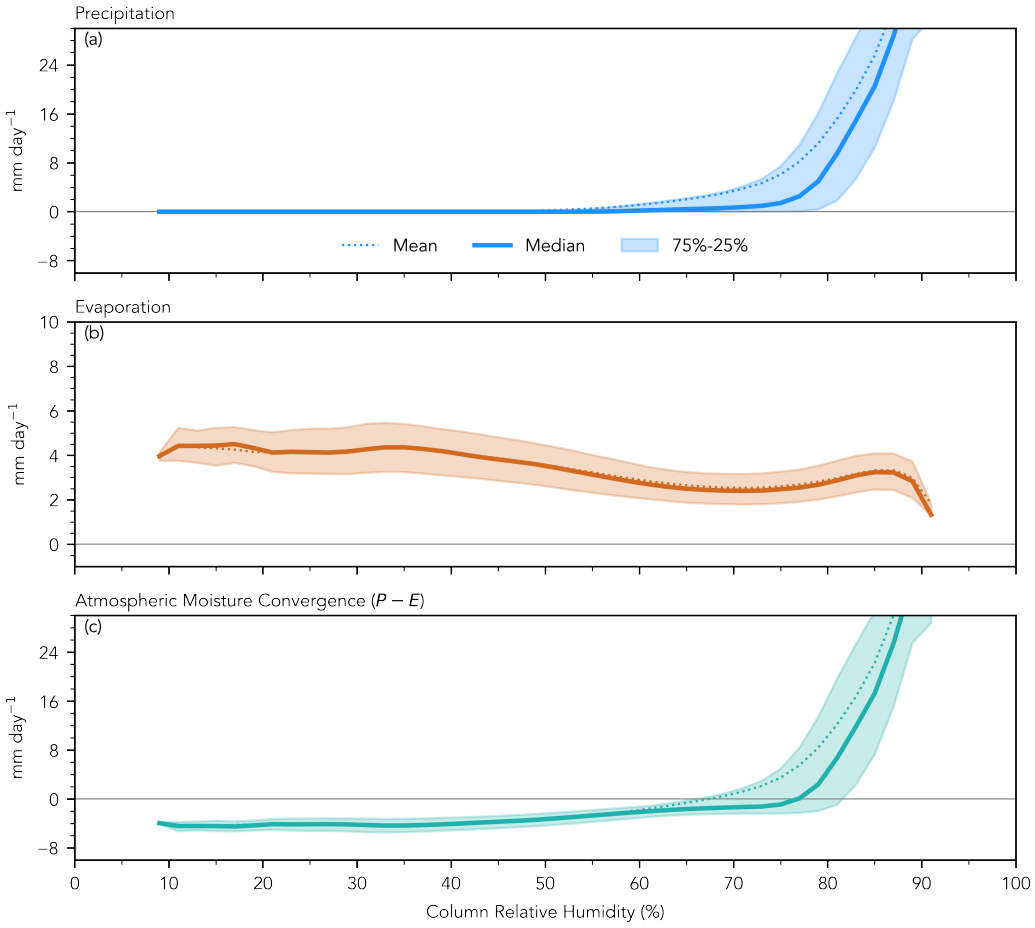

Figure 6. As in Fig. 5, but for the terms in the atmospheric moisture budget.

In addition to demonstrating that the ITCZ is a sink of moisture and a source of energy for the rest of the atmosphere, RM58 also realized this implied vertical transport within the ITCZ to balance the energy export. They noted that the mid-tropospheric minimum in moist static energy is not consistent with large-scale vertical energy transport. They instead proposed that convection provided the necessary transport because deep convective updrafts could lift energy to the upper levels of the atmosphere and bypass the moist static energy minimum. Recent work by Jenney et al. (2020) used a CRH analysis method similar to the one used in this study to show a shift to large-scale ascent, including environmental ascent, in extremely humid regions of these same RCEMIP simulations. In the following section, we explore the implications of large-scale ascent, in humid regions, and its effects on the vertical transports of moisture and energy

5 Moistening of the Troposphere Through Large-Scale Ascent

5.1 The Vertical Distribution of Static Energies

The transports of energy in the atmosphere can be understood using the dry static energy,

$$s = gz + c_p T, \tag{5}$$

and the moist static energy,

$$h = s + L_v q, \tag{6}$$

both of which are approximately conserved under adiabatic processes. In addition, the moist static energy is approximately conserved under condensation or evaporation.

The top row of Fig. 7 shows contours of the moist static energy as a function of altitude and CRH, with similar contours for the dry static energy and latent energy. The contours were constructed by calculating the area-weighted profile for each of the CRH bins of width 2%, which allows for the comparison of the vertical structure of each of the terms in Eq. 6 between dry and humid regions. The contours in panel a show the typical distribution of h in the tropics, in particular the mid-tropospheric minimum (marked by the black contour) as emphasized by RM58. The altitude where the minimum occurs

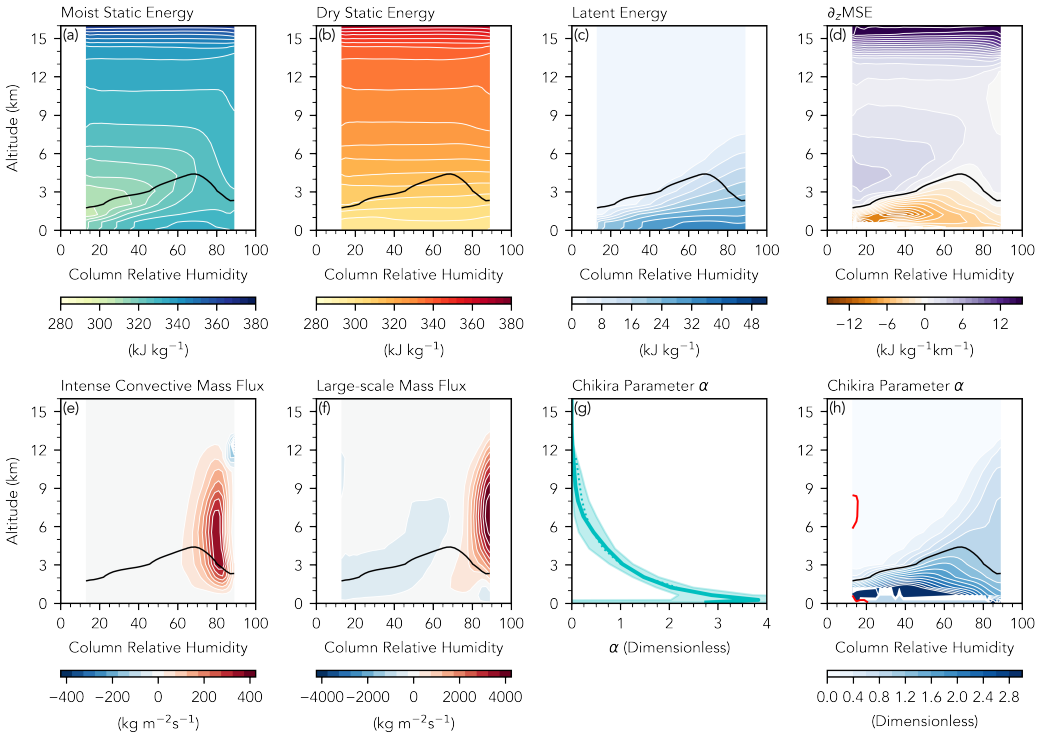

Figure 7. **a:** Profiles of moist static energy binned by the column relative humidity. **b-f** and **h:** Same as **a**, but for the dry static energy, the latent energy, the vertical moist static energy gradient, the convective-scale mass flux, the large-scale mass flux, and the Chikira parameter (α), respectively. In all panels except for **g**, the thick black line shows the level of the moist static energy minimum. In panel **h** the black contour also represents the level where α=1, and the red contour marks the level where $\alpha = 0$. Panel **g:** Domain-average profile of α.

depends on the CRH; it is near 2 km in dry regions, rises to near 5 km at 70% CRH, and then drops back to 2 km in extremely humid regions. In addition, the magnitude of the minimum depends on the CRH. This is illustrated in panel d, which shows contours of the vertical gradient of h. In dry regions the minimum is distinct, with relatively large values of the gradient above and below the minimum. However in humid regions the vertical gradient becomes weaker, especially above the minimum. As will be discussed later, this has important implications for the vertical transport for h.

The dry static energy (panel b) is largely independent of the CRH. This is unsurprising as the lack of rotation means that horizontal gradients of temperature are swiftly removed (Charney, 1963; Sobel et al., 2001). In contrast, panel c shows that the distribution of latent energy is strongly tied to the CRH. In dry regions water vapor is largely relegated to lower levels, but in humid regions water vapor extends through a much deeper layer of the troposphere. Comparison of panels b and c illustrates that the change in both the magnitude and altitude of the minimum are due to changes in latent energy rather than dry static energy. In fact, the weakening of in the minimum in h appears to be the result of a large quantity of water vapor above the altitude of the minimum, which also acts to reduce the vertical gradient.

The lifting of water vapor is a natural consequence of the shift to large-scale ascent in humid regions, as discussed by Jenney et al. (2020), and illustrated in panels e and f, which show the mass flux on convective and large scales. In panel e, "intense" refers to the mass flux calculated only when the CRM vertical velocity exceeds 2 ms^{-1}, following Jenney et al. (2020), while "large-scale" in panel f refers to the mass flux computed using the GCM vertical velocity. The intense convective mass flux maximizes near 80% CRH, but rapidly decreases in magnitude as the CRH continues to increase. In contrast, the large-scale mass flux shows weak descent through much of the domain and only becomes positive in the middle troposphere when the CRH exceeds 75%. As the CRH continues to increase the large-scale mass flux also increases in magnitude, reaching its largest value near 90%, the highest CRH value observed in the simulation.

5.2 Large-scale Ascent in Humid Regions

What causes this large-scale ascent that lifts water vapor in the troposphere? Ascent on convective sales is a buoyancy-driven process while large-scale ascent is driven

by large-scale heating. Evidently there is some heating in humid regions that drives this ascent. Chikira (2014) used the weak temperature gradient approximation (WTG, Charney (1963); Sobel et al. (2001)) to derive a form of the specific humidity equation,

$$\frac{\partial q}{\partial t} \simeq (\alpha - 1)\Big(C - E\Big) + \frac{\alpha}{L_v}\Big(Q_r + Q_i + Q_{df}\Big) + D_q + S_{df} + S_{hf}. \tag{7}$$

In Eq. 7, $C - E$ refers to the net rate of condensation minus re-evaporation. Q_r, Q_i, and Q_{df} represent the adiabatic heating due to radiation, liquid-ice phase changes, and vertical diffusion. D_q is the moisture tendency due to detrainment, while S_{df} and S_{hf} are moisture source terms representing sub-grid scale vertical diffusion and high-frequency waves. The condensation and heating terms in Eq. 7 are each multiplied by a parameter α, which is defined equivalently as

$$\alpha \equiv -\frac{L_v}{c_p \pi}\Big(\frac{\partial q}{\partial z}\Big)\Big(\frac{\partial \theta}{\partial z}\Big)^{-1} = -L_v\Big(\frac{\partial q}{\partial z}\Big)\Big(\frac{\partial s}{\partial z}\Big)^{-1} = 1 - \Big(\frac{\partial h}{\partial z}\Big)\Big(\frac{\partial s}{\partial z}\Big)^{-1}, \tag{8}$$

and determines the moisture tendency due to a particular source of heating. The mechanism for this moistening is straightforward: a localized heating induces large-scale rising motion, which can lift water vapor if the vertical moisture gradient (included in the definition of α) is large enough. In the case of the Q terms, any positive heating will tend to moisten the environment if α is positive. $C - E$ can moisten the environment, but only if α exceeds one. That is, ascent due to condensation heating can moisten the environment, but only if the vertical gradient of q is sharp enough to overcome the loss of water vapor to condensation.

In Eq. 7, WTG is used to diagnose the ascent (subsidence) associated with a particular heating (cooling). If the environmental conditions (specifically the vertical moisture gradient) are known, Eq. 7 quantifies the vertical moisture advection and by extension the moisture tendency of each heat source. This gives a method for decomposing the total moisture advection/tendency associated with different processes. Eq. 7 and related forms have been used in recent studies to investigate how different sources of heating contribute to the total vertical advection of moisture within the MJO (Chikira, 2014; Wolding & Maloney, 2015; Wolding et al., 2016; Janiga & Zhang, 2016; Wolding et al., 2017).

The domain average profile of α is shown in panel g of Fig. 7. Consistent with the profile of α presented by Chikira (2014), α is greater than unity in the lower troposphere. This means that any net heating will tend to moisten the atmosphere by inducing rising motion; including heating from condensation. Above the level where α passes through one, heating from condensation can no longer moisten as the conversion to condensed water dominates over any heating due to rising motion. However, moistening above this level can occur due to other types of heating, including radiative heating.

The contours in panel h of Fig. 7 show the vertical structure of α in dry and humid regions. As with the domain average profile, α is greater than unity in the lower troposphere in all regions. However there are several differences in the distribution of α between dry and humid regions. First, the $\alpha = 1$ contour does not occur at a fixed altitude, but varies between 2 to 5 km because it corresponds exactly to the altitude of the minimum of h, as can be inferred from Eq. 8. This indicates that heating due to condensation can account for some of the vertical motion in extremely humid regions, but *cannot* account for the vertical moisture transport above the minimum of h that is implied from the distribution of water vapor in panel c of Fig. 7. Above the minimum, some heat source other than condensation is required, with radiation as the obvious possibility. Typically, radiation does not heat the troposphere, as the longwave emission from water vapor is a strong net cooling. However as seen in panel c of Fig. 3, the integrated net heating rate becomes positive in humid regions, due to a strong longwave ACRE. In short, the ACRE can drive rising motion that lifts water vapor.

The radiative tendency profiles binned by the CRH are shown in the top row of Fig. 8. In dry regions the longwave tendency (panel a) is concentrated below 2 km, where the moist boundary layer favors radiative cooling from water vapor. As the CRH increases the distribution of water vapor becomes deeper (as shown above in Fig. 7.c) and the maximum in the longwave temperature tendency correspondingly shifts to higher altitudes. This culminates with a top-heavy longwave profile in humid regions, characterized by emission from the tops of clouds. This profile is accompanied by weaker longwave cooling in the lower troposphere, and also leads to a net *heating* in extremely humid regions.

The shortwave profile (panel b) is everywhere positive and mimics the longwave profile, shifting from a lower-level maximum in dry regions to an upper-level maximum in humid regions. When the longwave and shortwave tendencies are combined (panel c),

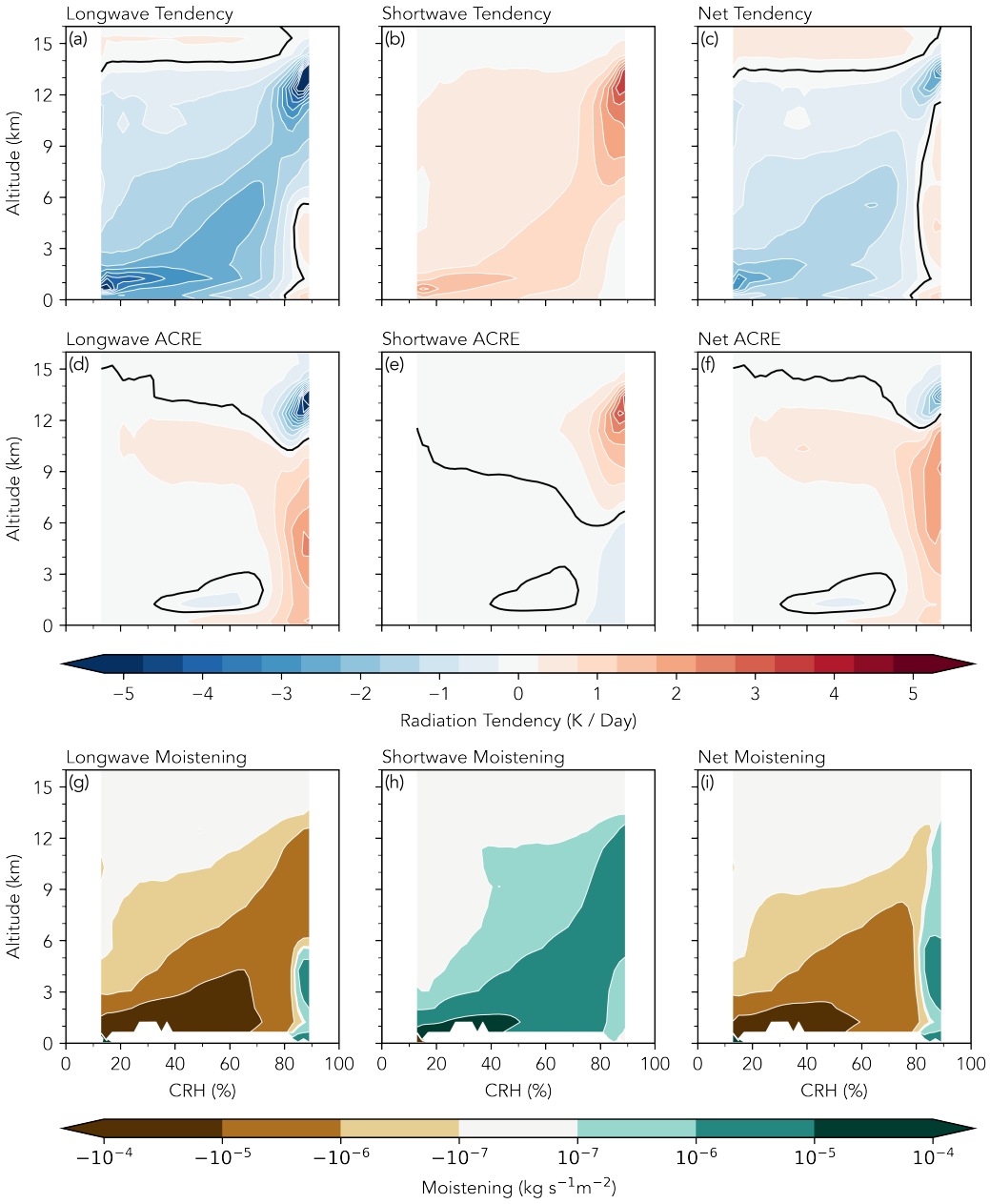

Figure 8. **a:** Vertically resolved longwave radiation tendency, binned by CRH. **b** and **c:** Same as **a**, but for the shortwave and net radiation tendencies. **d-f:** Same as **a-c**, but for the ACRE. In **a-f** the solid black line shows the zero contour. **g:** Moisture tendency due to longwave radiation, defined in the text. **h** and **i:** Same as **ga**, but for the moistening due to shortwave and net radiation. Note the logarithmic color scale for panels **g-i**.

the net profile is largely determined by the stronger longwave component and tends to cool the atmosphere. The exception is in humid regions, where the weak longwave heating below combined with shortwave heating aloft leads to a deep layer with a net positive radiation tendency.

The vertically integrated heating rates shown in Fig. 3 suggest that this heating is due to the ACRE rather than to clear-sky effects (e.g., not the result of changes to the distribution of water vapor), which is confirmed by looking the vertically resolved ACRE, shown in the middle row of Fig. 8. The longwave ACRE in panel d shows a strong heating through most of the troposphere in humid regions up to the level of cloud-top cooling. The shortwave ACRE (panel e) is strongly positive aloft in humid regions due to enhanced absorption of solar radiation by clouds, which leads to a slightly negative shortwave ACRE in lower levels of humid regions. The sum of the longwave and shortwave ACRE is positive through most of the troposphere in humid regions, and its structure is determined largely by the longwave contribution, as seen by comparing panels d and f. This positive ACRE is strong enough to change the sign of the radiation tendency and leads to a net radiative heating in humid regions, as seen in panel c.

To see how this net heating impacts the vertical advection of water vapor, the moistening of the troposphere due to radiation can be written using Eq. 7 as

$$\left(\frac{\partial q}{\partial t}\right)_r = \frac{\alpha}{L_v}\Big(Q_{rl} + Q_{rs}\Big), \tag{9}$$

where the subscript r refers to the moisture tendency due to radiation. Q_{rl} and Q_{rs} represent the longwave and shortwave heating rates (i.e., not the radiative tendencies). The bottom row of Fig. 8 shows the longwave, shortwave, and net moistening of the troposphere due to radiation, calculated using Eq. 9 and then binned by the CRH to give contours. As α is almost universally positive, the sign of the moisture tendency is determined entirely by the sign of the radiation terms. Because of this, radiation largely dries the atmosphere due to cooling-induced subsidence, but in humid regions the net radiative heating-induced ascent in moistens a deep layer of the troposphere in regions that are already quite humid.

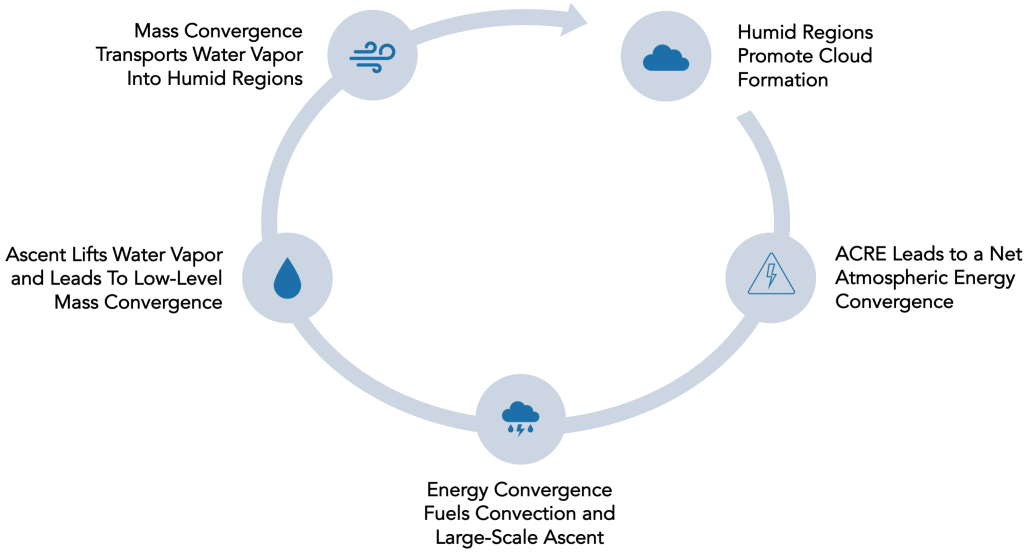

Figure 9. Diagram showing the cloud-longwave feedback described in the text

5.3 A Longwave-Cloud Feedback in the Tropics

Taken together our results suggest a cloud-longwave feedback that appears to be a fundamental characteristic of very humid regions in the tropics. First, clouds preferentially form in humid regions, where they absorb radiation, especially in the longwave. If the ACRE is large enough, it can lead to a net radiative heating throughout the depth of the troposphere. This heating then drives rising motion which lifts water vapor and homogenizes the moist static energy, making convective-scale ascent unnecessary for vertical energy transport. The rising motion also drives low-level moisture convergence (Neelin & Held, 1987), which transports water vapor from dry regions into humid regions, against the moisture gradient, in a way analogous to the description of the ITCZ from Riehl and Malkus (1958). This provides a steady source of moisture for regions that are already humid, supporting further cloud formation and completing a feedback loop. The steps of this feedback are summarized in Fig. 9.

6 Conclusion

We have performed an energy and moisture budget analysis of a set of GCM simulations configured in radiative convective equilibrium over a non-rotating ocean with uniform fixed SSTs and insolation. The results show that humid regions in these sim-

ulations export energy and import moisture in a way that is analogous to the ITCZ as first analyzed by Riehl and Malkus (1958), even though the simulations omit the ingredients necessary to form an ITCZ. We then analyzed the vertical structure of moist static energy, and found that the characteristic mid-tropospheric minimum becomes weak in humid regions, likely due to environmental-scale ascent (Jenney et al., 2020) which tends to make the moist static energy uniform in the vertical. Our analysis emphasizes the importance of the ACRE, especially its longwave component, in humid regions of the tropics. We find that the ACRE is strong enough to change the sign of the net radiation tendency in humid regions, and it is this heating which likely drives the large-scale ascent.

Our analysis describes a general tropical cloud-longwave feedback that exists even in this extremely idealized modeling framework. The feedback is similar to feedbacks that have been described elsewhere in the literature in a variety of contexts (as discussed in Section 1). Similar analysis performed on two sets of rotating aquaplanet experiments (one with super-parameterization, and one without) that include a meridional SST gradient and diurnal cycle yielded essentially identical results to those presented here (Needham, 2021).

Our study also supports the main conclusion of Needham and Randall (2021), namely that the ACRE depends on the CRH in a nonlinear way that is similar to the well-known behavior of precipitation, and that the ACRE as a function of the CRH is largely independent of the SST. This suggests that the longwave effect of tropical clouds is de-coupled from the SST, consistent with the fixed anvil temperature hypothesis (Hartmann & Larson, 2002; Zelinka & Hartmann, 2010)). The behavior of longwave cloud radiative effects in a warmer climate may instead be governed by changes in humidity. The PDFs of CRH in Fig. 2 show an increase in the probability of both extremely dry and extremely humid regions as the SST increases, with little change in the mean CRH (Tbl. 1). The increased frequency of humid regions would suggest an increase in grid cells with a large ACRE, while the increased frequency of dry regions would suggest the opposite. These competing effects complicate drawing simple conclusions about the mean behavior of longwave cloud radiative effects in a warmer climate, and may help to explain the non-monotonic relationship between SST and the top of atmosphere CRE as presented in Tbl. 1. These possibilities are left for future work.

Acknowledgments

This study utilized model output used originally by Jenney et al. (2020), which is available online (https://hdl.handle.net/10217/199724) as part of the Mountain Scholar institutional repository managed by Colorado State University.

References

Albern, N., Voigt, A., Buehler, S. A., & Grützun, V. (2018, August). Robust and nonrobust impacts of atmospheric Cloud-Radiative interactions on the tropical circulation and its response to surface warming. *Geophys. Res. Lett.*, *27*, 4937. Retrieved from `http://doi.wiley.com/10.1029/2018GL079599` doi: 10.1029/2018GL079599

Allan, R. P. (2011, September). Combining satellite data and models to estimate cloud radiative effect at the surface and in the atmosphere. *Met. Apps*, *18*(3), 324-333. doi: 10.1002/met.285

Arnold, N. P., & Randall, D. A. (2015, December). Global-scale convective aggregation: Implications for the Madden-Julian oscillation: GLOBAL-SCALE CONVECTIVE AGGREGATION. *J. Adv. Model. Earth Syst.*, *7*(4), 1499-1518. Retrieved from `http://doi.wiley.com/10.1002/2015MS000498` doi: 10.1002/2015ms000498

Benedict, J. J., Medeiros, B., Clement, A. C., & Olson, J. G. (2020, May). Investigating the role of cloud-radiation interactions in subseasonal tropical disturbances. *Geophys. Res. Lett.*, *47*(9), e2019GL086817. Retrieved from `https://onlinelibrary.wiley.com/doi/10.1029/2019GL086817` doi: 10.1029/2019gl086817

Bretherton, C. S., Blossey, P. N., & Khairoutdinov, M. (2005, December). An Energy-Balance analysis of deep convective Self-Aggregation above uniform SST. *J. Atmos. Sci.*, *62*(12), 4273–4292.

Bretherton, C. S., Peters, M. E., & Back, L. E. (2004). Relationships between water vapor path and precipitation over the tropical oceans. *J. Clim.*, *17*(7), 1517–1528.

Byrne, M. P., Pendergrass, A. G., Rapp, A. D., & Wodzicki, K. R. (2018, August). Response of the intertropical convergence zone to climate change: Location, width, and strength. *Curr Clim Change Rep*, *4*(4), 355-370.

Retrieved from http://dx.doi.org/10.1007/s40641-018-0110-5 doi: 10.1007/s40641-018-0110-5

Charney, J. G. (1963, November). A note on Large-Scale motions in the tropics. *J. Atmos. Sci.*, *20*(6), 607-609. Retrieved from https://doi.org/10.1175/1520-0469(1963)020<0607:ANOLSM>2.0.CO;2 doi: 10.1175/1520-0469(1963)020⟨0607:ANOLSM⟩2.0.CO;2

Chikira, M. (2014, February). Eastward-Propagating intraseasonal oscillation represented by Chikira–Sugiyama cumulus parameterization. part II: Understanding moisture variation under weak temperature gradient balance. *J. Atmos. Sci.*, *71*(2), 615–639.

Harrison, E. F., Minnis, P., Barkstrom, B. R., Ramanathan, V., & Gibson, G. G. (1990, October). Seasonal variation of cloud radiative forcing derived from the earth radiation budget experiment. *J. Geophys. Res.*, *95*(D11). Retrieved from https://www.researchgate.net/publication/23610598_Seasonal_variation_of_cloud_radiative_forcing_derived_from_the_Earth_Radiation_Budget_Experiment doi: 10.1029/JD095iD11p18687

Harrop, B. E., & Hartmann, D. L. (2016, April). The role of cloud radiative heating in determining the location of the ITCZ in aquaplanet simulations. *J. Clim.*, *29*(8), 2741-2763. Retrieved from https://doi.org/10.1175/JCLI-D-15-0521.1 doi: 10.1175/JCLI-D-15-0521.1

Hartmann, D. L., & Berry, S. E. (2017, May). The balanced radiative effect of tropical anvil clouds: Balance anvil clouds. *J. Geophys. Res. D: Atmos.*, *122*(9), 5003-5020. Retrieved from http://doi.wiley.com/10.1002/2017JD026460 doi: 10.1002/2017JD026460

Hartmann, D. L., & Larson, K. (2002, October). An important constraint on tropical cloud - climate feedback. *Geophys. Res. Lett.*, *29*(20), 12-1-12-4. Retrieved from http://doi.wiley.com/10.1029/2002GL015835 doi: 10.1029/2002GL015835

Janiga, M. A., & Zhang, C. (2016, June). MJO moisture budget during DYNAMO in a Cloud-Resolving model. *J. Atmos. Sci.*, *73*(6), 2257-2278. Retrieved from https://journals.ametsoc.org/view/journals/atsc/73/6/jas-d-14-0379.1.xml?tab_body=pdf doi: 10.1175/JAS-D-14-0379.1

Jenney, A. M., Randall, D. A., & Branson, M. D. (2020, May). Understanding the

response of tropical ascent to warming using an energy balance framework. *J. Adv. Model. Earth Syst.*.

Khairoutdinov, M. F., & Emanuel, K. (2018, December). Intraseasonal variability in a Cloud-Permitting Near-Global equatorial aquaplanet model. *J. Atmos. Sci.*, *75*(12), 4337-4355. Retrieved from `https://journals.ametsoc.org/view/journals/atsc/75/12/jas-d-18-0152.1.xml?tab_body=pdf` doi: 10.1175/JAS-D-18-0152.1

Khairoutdinov, M. F., & Randall, D. A. (2003, February). Cloud resolving modeling of the ARM summer 1997 IOP: Model formulation, results, uncertainties, and sensitivities. *J. Atmos. Sci.*, *60*(4), 607–625.

Li, Y., Thompson, D. W. J., & Bony, S. (2015, September). The influence of atmospheric cloud radiative effects on the Large-Scale atmospheric circulation. *J. Clim.*, *28*(18), 7263-7278. Retrieved from `https://journals.ametsoc.org/view/journals/clim/28/18/jcli-d-14-00825.1.xml?tab_body=pdf` doi: 10.1175/JCLI-D-14-00825.1

Medeiros, B., Clement, A. C., Benedict, J. J., & Zhang, B. (2021, March). Investigating the impact of cloud-radiative feedbacks on tropical precipitation extremes. *npj Climate and Atmospheric Science*, *4*(1), 1-10. Retrieved from `https://www.nature.com/articles/s41612-021-00174-x` doi: 10.1038/s41612-021-00174-x

Needham, M. R. (2021). *Links between atmospheric cloud radiative effects and tropical circulations* (Master's thesis, Colorado State University). Retrieved from `https://mountainscholar.org/handle/10217/100532`

Needham, M. R., & Randall, D. A. (2021, March). *Linking atmospheric cloud radiative effects, tropical precipitation, and column relative humidity.* Retrieved from `http://www.essoar.org/doi/10.1002/essoar.10506507.1` doi: 10.1002/essoar.10506507.1

Neelin, J. D., & Held, I. M. (1987). Modeling tropical convergence based on the moist static energy budget. *Mon. Weather Rev.*, *115*(1), 3–12.

Neelin, J. D., Peters, O., & Hales, K. (2009, August). The transition to strong convection. *J. Atmos. Sci.*, *66*(8), 2367-2384. Retrieved from `https://journals.ametsoc.org/view/journals/atsc/66/8/2009jas2962.1.xml` doi: 10.1175/2009JAS2962.1

Peters, O., & Neelin, J. D. (2006, May). Critical phenomena in atmospheric precipitation. *Nat. Phys.*, *2*(6), 393-396. Retrieved from https://www.nature.com/articles/nphys314 doi: 10.1038/nphys314

Popp, M., & Silvers, L. G. (2017, November). Double and single ITCZs with and without clouds. *J. Clim.*, *30*(22), 9147-9166. Retrieved from https://doi.org/10.1175/JCLI-D-17-0062.1 doi: 10.1175/JCLI-D-17-0062.1

Powell, S. W. (2019, December). Observing possible thermodynamic controls on tropical marine rainfall in moist environments. *J. Atmos. Sci.*, *76*(12), 3737-3751. Retrieved from https://journals.ametsoc.org/view/journals/atsc/76/12/jas-d-19-0144.1.xml doi: 10.1175/jas-d-19-0144.1

Ramanathan, V., Cess, R. D., Harrison, E. F., Minnis, P., Barkstrom, B. R., Ahmad, E., & Hartmann, D. L. (1989, January). Cloud-Radiative forcing and climate: Results from the earth radiation budget experiment. *Science*, *243*(4887), 57-63.

Randall, D. A., DeMott, C., Stan, C., Khairoutdinov, M., Benedict, J., McCrary, R., ... Branson, M. (2016, April). Simulations of the tropical general circulation with a multiscale global model. *Meteorol. Monogr.*, *56*, 15.1–15.15.

Randall, D. A., Harshvardhan, Dazlich, D. A., & Corsetti, T. G. (1989, July). Interactions among radiation, convection, and Large-Scale dynamics in a general circulation model. *J. Atmos. Sci.*, *46*(13), 1943-1970. Retrieved from https://journals.ametsoc.org/jas/article/46/13/1943/22282/Interactions-among-Radiation-Convection-and-Large doi: 10.1175/1520-0469(1989)046⟨1943:IARCAL⟩2.0.CO;2

Raymond, D. J. (2000, July). Thermodynamic control of tropical rainfall. *Q.J.R. Meteorol. Soc.*, *126*(564), 889-898. Retrieved from http://doi.wiley.com/10.1002/qj.49712656406 doi: 10.1002/qj.49712656406

Raymond, D. J., Sessions, S. L., Sobel, A. H., & Fuchs, Ž. (2009, March). The mechanics of gross moist stability. *J. Adv. Model. Earth Syst.*, *1*(3). Retrieved from http://doi.wiley.com/10.3894/JAMES.2009.1.9 doi: 10.3894/JAMES.2009.1.9

Raymond, D. J., & Zeng, X. (2005, April). Modelling tropical atmospheric convection in the context of the weak temperature gradient approximation. *Quart. J. Roy. Meteor. Soc.*, *131*(608), 1301-1320. Retrieved from http://doi.wiley

.com/10.1256/qj.03.97 doi: 10.1256/qj.03.97

Riehl, H., & Malkus, J. S. (1958). On the heat balance in the equatorial trough zone. *Geophysica*, *6*, 503–537.

Ruppert, J. H., Jr, Wing, A. A., Tang, X., & Duran, E. L. (2020, November). The critical role of cloud-infrared radiation feedback in tropical cyclone development. *Proc. Natl. Acad. Sci. U. S. A.*, *117*(45), 27884-27892. Retrieved from http://dx.doi.org/10.1073/pnas.2013584117 doi: 10.1073/pnas.2013584117

Rushley, S. S., Kim, D., Bretherton, C. S., & Ahn, M.-S. (2018, January). Re-examining the non-linear moisture-precipitation relationship over the tropical oceans. *Geophys. Res. Lett.*, *45*(2), 1133-1140. doi: 10.1002/2017GL076296

Sherwood, S. C., Ramanathan, V., Barnett, T. P., Tyree, M. K., & Roeckner, E. (1994). Response of an atmospheric general circulation model to radiative forcing of tropical clouds. *J. Geophys. Res.*, *99*(D10), 20829. doi: 10.1029/94jd01632

Slingo, A., & Slingo, J. M. (1988, July). The response of a general circulation model to cloud longwave radiative forcing. i: Introduction and initial experiments. *Q.J Royal Met. Soc.*, *114*(482), 1027-1062. doi: 10.1002/qj.49711448209

Sobel, A. H., Nilsson, J., & Polvani, L. M. (2001, December). The weak temperature gradient approximation and balanced tropical moisture waves. *J. Atmos. Sci.*, *58*(23), 3650-3665. Retrieved from https://doi.org/10.1175/1520-0469(2001)058<3650:TWTGAA>2.0.CO;2 doi: 10.1175/1520-0469(2001)058⟨3650:TWTGAA⟩2.0.CO;2

Stevens, B., Bony, S., & Webb, M. (2012, September). *CLOUDS ON-OFF KLIMATE INTERCOMPARISON EXPERIMENT (COOKIE).* http://www.euclipse.eu/wp4/wp4.html. Retrieved from http://www.euclipse.eu/wp4/wp4.html (Accessed: 2020-7-28)

Voigt, A., & Albern, N. (2019, December). No cookie for climate change. *Geophys. Res. Lett.*, *46*(24), 14751-14761. Retrieved from https://onlinelibrary.wiley.com/doi/abs/10.1029/2019GL084987 doi: 10.1029/2019GL084987

Wing, A. A., & Emanuel, K. A. (2014, March). Physical mechanisms controlling self-aggregation of convection in idealized numerical modeling simulations. *J. Adv. Model. Earth Syst.*, *6*(1), 59–74.

Wing, A. A., Reed, K. A., Satoh, M., Stevens, B., Bony, S., & Ohno, T. (2018, March). Radiative–convective equilibrium model intercomparison project. *Geoscientific Model Development*, *11*(2), 793–813.

Wing, A. A., Stauffer, C. L., Becker, T., Reed, K. A., Ahn, M., Arnold, N. P., ... Zhao, M. (2020, July). Clouds and convective Self-Aggregation in a Multi-Model ensemble of Radiative-Convective equilibrium simulations. *J. Adv. Model. Earth Syst.*. Retrieved from https://onlinelibrary.wiley.com/doi/abs/10.1029/2020MS002138 doi: 10.1029/2020MS002138

Wolding, B. O., Dias, J., Kiladis, G., Ahmed, F., Powell, S. W., Maloney, E., & Branson, M. (2020, May). Interactions between moisture and tropical convection. part i: The coevolution of moisture and convection. *J. Atmos. Sci.*, *77*(5), 1783-1799. Retrieved from https://journals.ametsoc.org/view/journals/atsc/77/5/jas-d-19-0225.1.xml doi: 10.1175/jas-d-19-0225.1

Wolding, B. O., & Maloney, E. D. (2015, October). Objective diagnostics and the Madden–Julian oscillation. part II: Application to moist static energy and moisture budgets. *J. Clim.*, *28*(19), 7786-7808. Retrieved from https://journals.ametsoc.org/view/journals/clim/28/19/jcli-d-14-00689.1.xml doi: 10.1175/JCLI-D-14-00689.1

Wolding, B. O., Maloney, E. D., & Branson, M. (2016, December). Vertically resolved weak temperature gradient analysis of the madden- julian oscillation in SP-CESM. *J. Adv. Model. Earth Syst.*, *8*(4), 1586-1619. Retrieved from https://onlinelibrary.wiley.com/doi/abs/10.1002/2016MS000724 doi: 10.1002/2016ms000724

Wolding, B. O., Maloney, E. D., Henderson, S., & Branson, M. (2017, March). Climate change and the Madden-Julian oscillation: A vertically resolved weak temperature gradient analysis. *J. Adv. Model. Earth Syst.*, *9*(1), 307-331. Retrieved from http://doi.wiley.com/10.1002/2016MS000843 doi: 10.1002/2016ms000843

Zelinka, M. D., & Hartmann, D. L. (2010, August). Why is longwave cloud feedback positive? *J. Geophys. Res.*, *115*(D16), 1606. Retrieved from http://doi.wiley.com/10.1029/2010JD013817 doi: 10.1029/2010JD013817